Characterization of a solar cell by varying illumination

Andrzej Kołodziej[a*], Michał Kołodziej[b]

[a] *University of Applied Sciences in Tarnow, Polytechnic Faculty, Department of Electronics, Telecommunications and Mechatronics, ul. Mickiewicza 8, 33-100 Tarnów, Poland*
[b] *Private scientific activity, Kraków, Poland*

Article history
Received: 27 November 2020
Received in revised form:
21 January 2021
Accepted: 26 January 2021
Available online: 31 January 2021

Abstract
This work aims to confirm that the single-diode model of a monocrystalline cell can be used successfully also for thin-film solar cells when their basic parameters are calculated using the method of changing illumination. The authors describe the experimental procedure, in which I–V curves of thin-film solar cells are measured when illumination levels are changing. In experiments, a fully reflective 500 W solar simulator is used as an excellent broadband white light source, which provides the range of 0.01–10 Sun settings.

Keywords: thin films, solar cell measurement, silicon, I–V characteristic, varying illumination

Introduction

Successful innovation and development programs of solar PV technology depend on effective understanding and control of all issues contributing to performance, manufacturability, long-term reliability, and lifecycle cost of commercial solar cells. In literature, it is possible to find [1–7] many different models of solar cells and methods for stating their performance parameters. Thin-film photodiodes or solar cells may have different structures. One simplified version of the most widely used superstrate structure is shown in Fig. 1. This structure is a good example of p-i-n thin-film silicon solar cells. In such p-i-n devices, the intrinsic absorber layer is the space charge zone, when the carrier transport is performed by drift, not by diffusion.

The mobility-lifetime product $\mu\tau$ is now the key parameter determining effective carrier recombination. The average distance covered by a carrier before recombining is given by $\mu\tau E$, where E is the present electric field.

Fig. 2 presents the current-voltage (I–V) characteristics for the p-i-n photodiode and also the p-i-n solar cell in three states: in the dark, after the initial illumination and after the prolonged illumination. The I–V characteristics are plotted in three quadrants of the I–V coordination system. In the first and fourth quadrants, the direct polarization of a diode is shown, while in the third quadrant – in the reverse direction. In the fourth quadrant, the photodiode works as a generator of current, i.e. as a solar cell. Some degradation phenomena can also be observed in thin-film solar cells after many hours of operation.

The current-voltage characteristic of a solar cell or a module is useful because it is sensitive to many module design issues, such as spectral response, interconnection problems, optical alignment effects, thermal management issues, bypass diode faults, and parasitic impedances [6–9]. The I–V reflects the changes in the distribution of the gap states in the space charge zone of a solar cell under long-term illumination [9]. Information extracted from I–V curve is a crucial step in the modelling and simulation of solar cells, solar panels and solar systems [5–14].

In the paper, the Authors propose the experimental procedure of I–V curve measurement after short and defined changing of illumination levels, according to [9, 12, 15–20]. The aim of the experiment is:

- to show empirically, that the equivalent circuit of a single diode shown in Fig. 3 describes quite well the experimentally measured electrical behaviour of illuminated solar cells shown in Figs. 4–7, even when illumination levels are changing up to six orders of magnitude;
- to answer for which illumination the recombination losses influence the I–V curve so that the simplified equivalent model from Fig. 3 cannot be used.

* Corresponding author: a_kolodziej@pwsztar.edu.pl

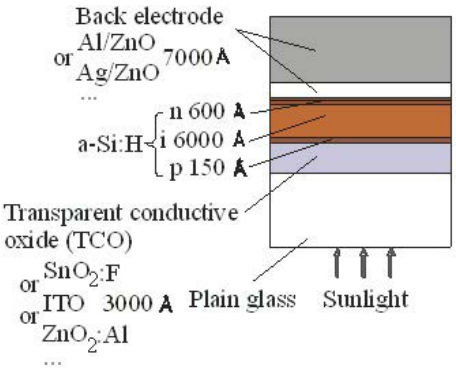

Figure 1. The basic structure of a typical p-i-n thin-film silicon solar cell in a superstrate configuration.

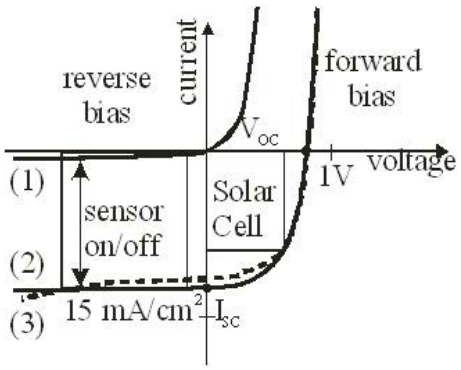

Figure 2. Schematic characteristics of p-i-n microcrystalline Si:H photodiode: (1) the dark state, (2) the initial illuminated state and (3) the state after prolonged light illumination. It is seen that the initial ISC and fill factor decrease after illumination. The solar cell sensor regimes and a forward regime are indicated.

Experiment and model. Light and dark I–V solar cell characteristics

Solar cell parameters such as short circuit current (I_{SC} – output current at $V = 0$), open-circuit voltage (V_{OC} – output voltage at $I = 0$), current and voltage at maximum power point (U_{PMAX}, I_{PMAX}) are usually found directly from I–V curve under the illumination. Other important parameters such as photo-generated current (I_{PH}), series resistance (R_S), shunt resistance (R_{SH}), and diode characteristics are determined from the equivalent model of the solar cell. There are two equivalent circuits (see Fig. 3), and an adequate mathematical description of characteristics I–V for crystalline and thin-film solar cells is given elsewhere [11–17]. Typically, the output I–V characteristic curve of a crystalline silicon solar cell under the illumination can be represented, either by a simpler single diode model with a single dominant current transport mechanism, or a more accurate double diode model with two different current transport mechanism, derived from Kirchhoff's first law (i.e., $0 = I_{ph} - I_{D1} - I_{D2} - I_{SH} - I$), given by the equation:

$$I = I_{ph} - I_{S1}\left[\exp\left(\frac{V + IR_S}{n_1 V_t}\right) - 1\right] - I_{S2}\left[\exp\left(\frac{V + IR_S}{n_2 V_t}\right) - 1\right] - \frac{V + IR_S}{R_{SH}} \quad (1)$$

where:

I – output current at the illumination, I_{PH} – photo-generated current, I_S – diode saturation current, n – diode ideality factor, V_t – thermal voltage, V – output voltage, R_S – series resistance, R_{SH} – shunt resistance, I_{S1}, I_{S2} – diode 1, 2 (D1, D2) saturation currents, n_1, n_2 – diode 1, 2 ideality factor, respectively.

Equation (1) is related to the solar cell behaviour under the illuminating photon flux, and is referred to as "photovoltaic output characteristic (or illuminated I–V characteristic)". The light I–V characteristic is obtained in the fourth quadrant of the plane – the solar cell acts as a generator in this case.

The dark I–V characteristic can be used to find specific solar cell parameters. The output current-voltage dependence in this manner assumes no external light illumination, and the solar cell is tested as a single diode (or two diodes) load supplied by dc power from an external bias supply. In this case, the characteristic falls into the first quadrant of the current-voltage plane and differs from the photovoltaic output characteristic by the absence of the light-generated current and by the reverse direction of the output current, as illustrated by Fig. 3.

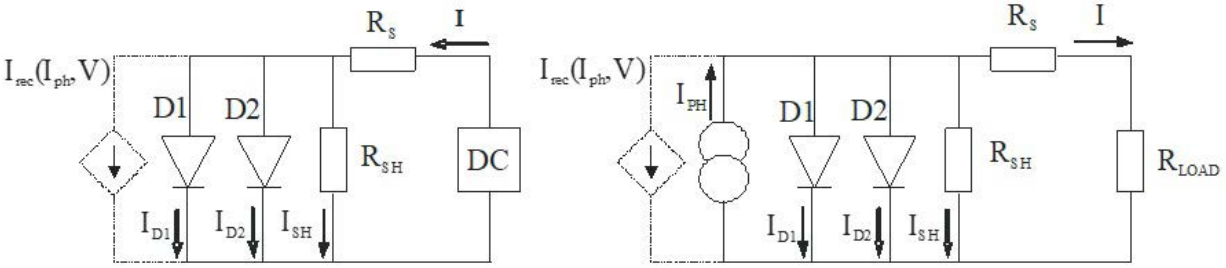

Figure 3. Two diode equivalent model with corresponding currents (single diode equivalent model uses one diode). The light I–V characteristic is obtained by measuring the solar voltage across the solar cell terminals and the current through the resistive load (R_{LOAD}) – right side of the figure. The dark I–V characteristic is obtained in a similar way – dc power supply tests the solar cell without application of any illumination ($I_{PH} = 0$) – left side of the figure. I_{D1}, I_{D2} – current through diode D_1, D_2, I_{SH} – current through shunt resistance, I_{rec} – recombination current.

In the case of thin silicon solar cells (amorphous and microcrystalline), the usual superposition principle stating that the J-V curve under illumination may be obtained just by shifting the dark characteristic upwards is not valid. Generally speaking, recombination is relatively intense within the intrinsic layer of the disordered semiconductor. Therefore it is reasonable to describe the situation by introducing an additional recombination loss term I_{rec} into the equivalent circuit, a term symbolized by the current sink in Fig. 3. This especially confirms itself in the case of the Staebler-Wronski effect SWE. The mobility lifetime product $\mu\tau_{EF}$ is now the key parameter determining effective carrier recombination. Generally, this dependence is complex and difficult to describe and solve. This can be symbolically written as:

$$I = I\left(I_{ph}, I, V, \mu\tau\left(I_{ph}, V, time\right)\right) \quad (2)$$

Undoubtedly, the solution of equation (2) requires case-specific simplifications and complex iterative procedures. For the measurements, the author has developed the system described in [8]. The 500W fully reflective solar simulator makes an excellent broadband white light source bias as it complies with ASTM E927-05(2005) and IEC-904-9 standards for solar cell testing. This means that it is capable of achieving up to 2 Suns (200 mW/cm^2) of light intensity using an AM1.5G filter on a 5 cm x 5 cm area within industry recognized spatial uniformity, temporal stability, and spectral match characteristics for solar cell testing. The AM1.5G filter and thermopile broadband detector are two important features of this solar simulator. To vary 0.01–2 Sun settings, a combination of both neutral density filters and variable focus option is needed.

The standard I–V test measurement system has a maximum limit of 20W measured power from the solar cell with the current generated, not exceeding 1A. This limit is imposed by the Keithley 2400 source meter. The I–V measurement system sweeps the I–V curve with an automatically adjustable resistive load and records multiple I–V data points along the way. The voltage and current ranges are software selectable, and so is the number of points taken, which is typically from 10 to 200 points, depending on the time allowed for the test. The I–V data point values are then recorded and plotted on a computer display and saved in an ASCII text file [8].

Results and discussion. I–V curve with varying illumination

The procedure for solar cell characterization is proposed, consisting of measurement of the I–V curve at a given level of illumination as, for example, is shown in Fig. 5 and also in Fig. 4 and 6. The results can be summarized into six characteristic parameters, as follows: 1) the short circuit current I_{sc}; 2) the open-circuit voltage V_{oc}; 3) the fill factor FF; 4) the efficiency η; 5) the "open-circuit resistance" $R_{oc} = (\partial V/\partial I)_{I=0}$, which can be connected with the series resistance R_s; 6) and the "short circuit resistance" $R_{sc} = (\partial V/\partial I)_{V=0}$, which can be connected with the shunt resistance R_{SH}.

The latter two parameters, R_{OC} and $R_{SC,}$ are the key factors for the current approach; they are the reciprocal slopes of the I–V curve.

The basic idea relies on I–V curve measurement in a wide range of illumination levels, rather than at constant illumination level e.g. 100 W/m^2. In that way, additional information about the device can be acquired.

The experimental results are drawn as a function of the short circuit current I_{sc} or the open-circuit voltage V_{oc} omitting, in this way, the need for calibrating illumination levels.

This has been made with the data calculated after the measurements of the laboratory solar cell made by the Authors. It was a single-junction thin-film solar cell with the following structure: glass/ITO/ZnO/p-i-n silicon film with the *i*-layer thickness of d_i = 0.35 μm /ZnO/Ag. The initial average efficiency of the cell was 8.2%. The experimental data are presented in Fig. 5, and the calculated results are shown in Fig. 4. The experimental data from Fig. 5 are schematically presented in Fig. 6. The degraded by the Red Sun characteristics and then heated in a special recovery process are shown in Fig. 7 [8].

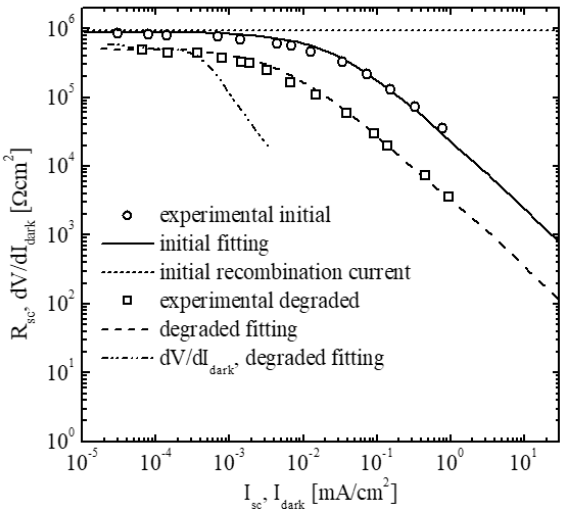

Figure 4. The method of analysis of $R_{SC} = d_V / dI_{dark}$ from the dependence of I–V parameters on the illumination intensity is shown. The experimental points are the author's data for a single junction. Avoiding the recombination current dotted line gives only the expectation for R_{SC}. I_{sc} is under AM1.5. The dash-dot-dot line d_V / dI_{dark} is a function of I_{dark}.

Introducing the simplified recombination formula into the single diode equivalent circuit, the following expression can be obtained:

$$I(V) = -I_{ph} + I_{ph} \cdot \frac{d_i^2}{(\mu\tau)_{eff}\left[V_{bi} - (V - IR_s)\right]} + \\ + I_0\left(e^{(V-IR_s)/(nkT/e)} - 1\right) + \frac{V - IR_s}{R_{SH}} \tag{3}$$

The photogenerated current, I_{ph}, is reduced by the loss currents caused by recombination in the *i*-layer, by the diode with its saturation current, I_0, and its quality factor n (*e* denotes here the elementary charge, *k* – Boltzmanns' constant, *T* – the absolute temperature of the device) and by the shunt resistance R_{SH}.

It is assumed that this model will operate for small forward voltages only, where the approximate assumptions mentioned above can be considered to be fulfilled.

This is the case in the short circuit area [8] and it is met at Eq. 3 that the slope R_{sc} is specified by the recombination conditions in the model.

$$\mathrm{R_{sc}} = \mathrm{I_{ph}^{-1}} \cdot \frac{(\mu\tau)_{\mathrm{eff}}\,\mathrm{V_{bi}^2}}{\mathrm{d_i^2}} \tag{4}$$

Here the R_s and R_{SH} influence has been neglected, which is correct for middle illumination levels. The R_{sc} measurement delivers direct information about the effective $(\mu\tau)_{eff}$– product inside the *i*-layer of the device.

Numerical simulation of amorphous silicon solar cells achieved by means of the programme described in [8] with the use of a standard defect model shows that the recombination current inside the *i*-layer is the loss current demonstrating the strongest change with the external voltage according to [8, 12, 15].

Other loss currents (e.g. those connected with recombination at the interfaces between the intrinsic and the doped layers) show a very weak dependence on the external voltage, which suggests that the influence on R_{sc} may be neglected.

The built-in voltage of amorphous silicon solar cells is $V_{bi} = 0.88\ V$, as determined by the Authors, and this value was used for the subsequent calculations.

The assumption that V_{bi} is invariable during degradation allows, by monitoring R_{sc}, for direct measurement of the degradation state in the device's *i*-layer.

In the open-circuit region, the model loses its validity as the underlying theoretical assumptions are no longer fulfilled. It is, therefore, surprising how sometimes the open-circuit voltage of the non-degraded cell matches that of the model. The validity of the model can also be seen from it matching well to the explicit I–V curves shown in [8, 13].

The model for thin-film silicon solar cells and modules presented in Eq. (3) allows for six regimes of illumination levels to be distinguished. These are shown in Fig. 5 and schematically marked in Fig. 6:

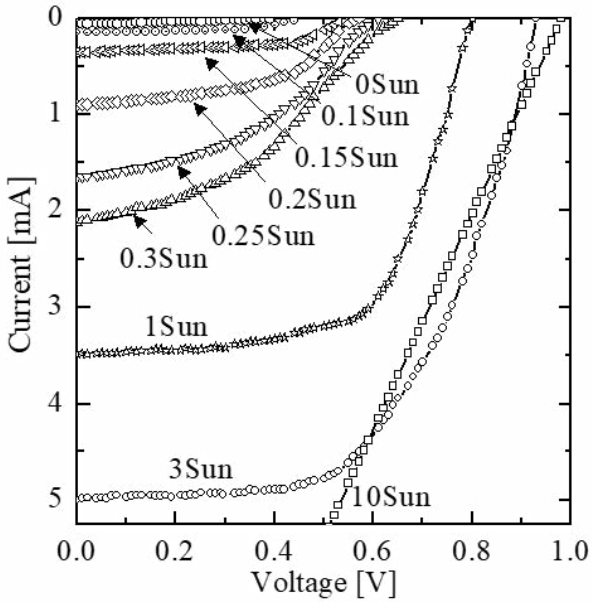

Figure 5. I–V characteristics of a cell made by the author for different lighting. They are the subject of the analyzes presented below and schematically summarized in Fig. 6.

1. At the lowest illumination levels, the I–V curve of the solar cell is dominated by its shunt resistance, R_{SH}, leading to a linear I–V curve, as sketched in Fig. 6.1. Both R_{oc} and R_{sc} are equal to the shunt resistance, R_{SH}. This case is characterized by the independence of R_{sc} and R_{oc} from the illumination: such behaviour can be observed on the left side of Fig. 6.1. In this illumination case, the low shunt resistance, R_{SH}, leads to a reduced open-circuit voltage V_{oc}, as well as to a fill factor FF of 0.25. The lower the value of R_{SH}, the higher the illumination level has to be in order to ensure that the performance of the device is not affected by R_{SH}. The detection of the shunt resistance in this illumination regime may be used for the quality control of commercial amorphous silicon solar modules.
2. At the increased illumination level, the shunt resistance R_{SH} only dominates the short circuit part of the I–V curve, as shown in Fig. 6.2 and 6.3. The fill factor FF is still reduced by R_{SH}, but the open-circuit voltage V_{oc} is no longer affected. The inverse slope R_{sc} is still equal to the shunt resistance R_{SH}, whereas R_{oc} is determined by the physics of the junction.
3. In this case, neither the series nor the shunt resistance R_{SH} affects the I–V curve of the device (Fig. 6.3). Both the slopes R_{oc} and R_{sc} are determined by the physics of the p-i-n

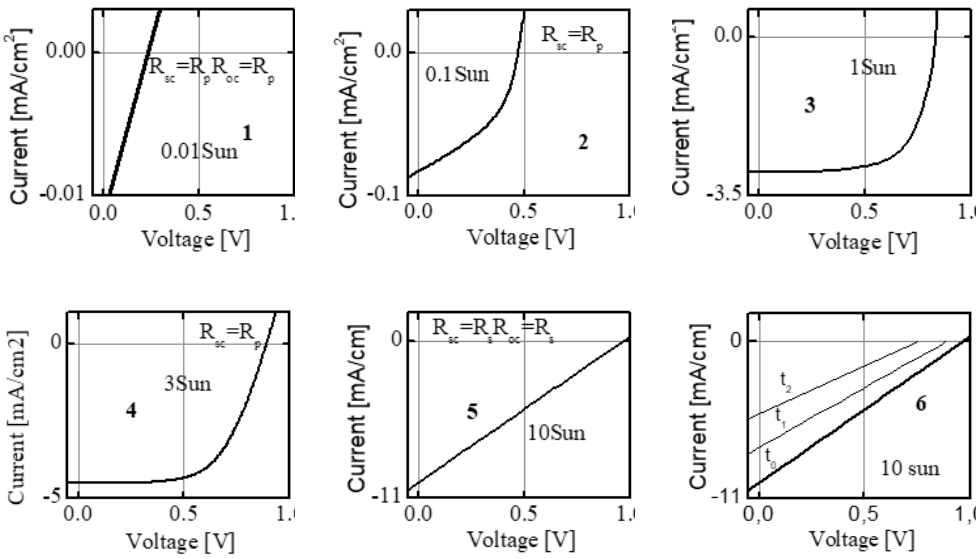

Figure 6. Examples of approximate I–V characteristics for different illumination levels are shown. Internal figures 6.1 to 6.5 show varying I–V curves at illumination levels from 0.01 to 10 Sun, and figure 6.6 shows the degradation of the I–V curve for an amorphous solar cell after prolonged exposure. The results correspond to the approximations of equation (3), and the experimental characteristics shown in Fig. 5. R_{oc} reflects the physics of the p-i-n junction in cases 2) and 3 (in Fig. 6.2 and in Fig. 6.3). In cases 3 and 4 (in Fig. 6.3 and in Fig. 6.4), R_{sc} is determined by the recombination in the *i*-layer, see also Eq. (4).

junction and R_{sc} may be used to assess the recombination in the *i*-layer Eq. (4). In this case, the fill factor *FF* exhibits the best values; a fact which makes case 3 recommendable for the practical operation of amorphous silicon solar cells or modules. This is the only case where the fill factor *FF* correctly indicates the state of device degradation.

4. Under the illumination level increased further the series resistance R_s of the device begins to affect the open circuit region of the I–V curve, as indicated schematically in Fig. 6.4. Thereby, the open circuit voltage V_{oc} is unaffected; however, the open-circuit resistance R_{oc} is now determined by the series resistance R_s. This leads to a reduced fill factor *FF*. The short circuit region, and especially R_{sc}, are not affected by R_s. This regime is not reached pointly by the laboratory cell shown in Fig. 5 and 6, because of its low series resistance, but it is mostly achieved by commercial modules under one Sun illumination. It is characterized by the flattening of the dependence of R_{oc} on the illumination level.
5. At the highest illumination levels, the I–V curve predicted by the model is completely dominated by the series resistance R_s, leading to a linear I–V curve with a fill factor *FF* of 0.25 (Fig. 5, 6). In this case, the inverse slopes R_{oc} and R_{sc} are equal to the series resistance R_s of the device.
6. Analysis in the case of long-term illumination and illumination with red light in the range of 600–700 nm, which enables the role of the rear reflector to be studied. This illumination effectively degrades photoconductivity and dark conductivity in the deep regions of the cell (that is, not only covering the p – i area). Changes in the light characteristics of the cell are visible over time. It is seen in Fig. 2. These changes are also visible in the dark current analysis in Fig. 7.

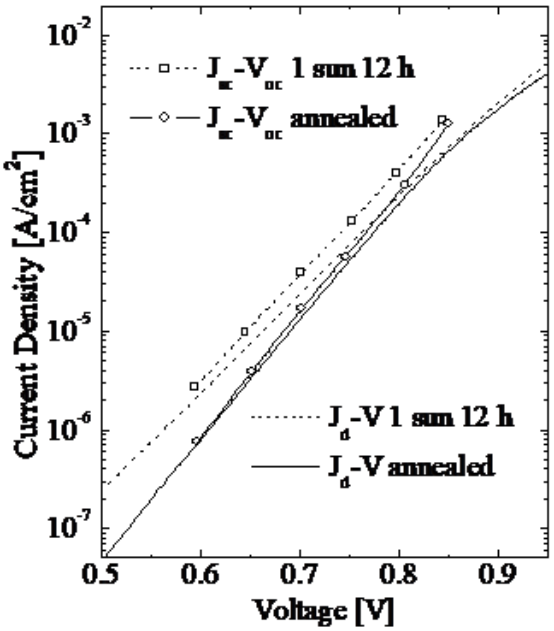

Figure 7. Plots of J_{sc} as a function of V_{oc} and J_d as a function of V, for the p-i-n cell with the −*i*-layer of the thin silicon. This is the same cell as analyzed in Fig. 4 and 6, before and after the degradation with red light, 550 nm filter of Sun, of intensity 100 mW/cm^2. The degradation was carried out with red light due to its penetration depth. The annealing process partially reversed the degradation [author's data] [8, 13].

For the intermediate illumination case 3, where the effects of the series and shunt resistance (R_s, R_{SH}) can be neglected, the analytical model [Eq. (3)] yields the following expression:

$$V_{oc} = \frac{nkT}{e} \ln\left(\frac{I_{sc}}{I_0}\right) \tag{5}$$

Here, the effect of the recombination losses in the *i*-layer is also neglected. Fitting this equation to the logarithmic region of the measured V_{oc}-I_{sc}-*behaviour* [Eq. (5)] , (Fig. 4 and 6) yields the diode saturation current I_0 and the quality factor, n.

The high illumination limit of R_{oc} is, according to the model, equal to the series resistance, R_s, which may be taken as the asymptotic saturation value of R_{oc} (cases 4 and 5). The series resistance, R_s, is physically determined by the sheet resistance of the electrodes, especially that of the transparent electrode.

The low illumination limit of R_{sc} is, according to the model, equal to the shunt resistance R_{SH}, which may be taken as the asymptotic saturation value of R_{sc} (cases 2 and 1). R_{SH} may also be determined by the saturation of the slope ($\partial V / \partial I_{dark}$) for low dark currents, I_{dark} (see the dash-dot-dot line in Fig. 4 and 6, note that low dark currents – here less than 3×10^{-4} mA/cm^2 – are determined by R_{SH} and not by the p-i-n-junction). The shunt resistance R_{SH} is a measure of the technological quality of the device: low values of R_{SH} indicate high leakage currents due to p-i-n holes.

The $(\mu\tau)_{eff}$ product is the key parameter that characterizes the new recombination term in the model and is determined from the power-law regime of the experimental $R_{sc}(I_{sc})$ data (case 3, see Fig. 4 and 6 using Eq. (4). The built-in voltage V_{bi} can be assumed to be approximately 0.88 V (for a more precise but rather cumbersome experimental determination of V_{bi} see [3] or [4]).

Conclusions

The I–V characteristics of thin-film cells can be analyzed using "the short time" single-diode model, observing the boundary conditions determining the areas of possible approximations. They have been analyzed in this paper and they relate to the appropriate levels of light intensity, voltage, and measurement current mainly in the fourth quadrant. This requires knowledge of the physics of the diode surface and bulk, especially in the case of thin-film cells. In the case of long-term lighting, measurements require knowledge of the nature of the Staebler-Wronski effect (SWE) [9].

Acknowledgment

The work was supported by the NCN contract no. NCN/2011/01/B/ST7/06005, and internal grant of the University of Applied Sciences in Tarnow no BAD-011/2019, under the agreement PWSZ/PRWRs/0700-11/PNU/2019.

Author Contributions

Conceptualization, Andrzej Kołodziej; methodology, Andrzej Kołodziej, Michał Kołodziej; software, Andrzej Kołodziej, Michał Kołodziej; investigation, Andrzej Kołodziej, Michał Kołodziej; data curation, Michał Kołodziej; writing—original draft preparation, Andrzej Kołodziej; writing—review and editing, Michał Kołodziej; project administration, Andrzej Kołodziej; funding acquisition, Andrzej Kołodziej.

References

1. Sze SM. Physics of semiconductor devices. New York: Wiley Interscience; 1969.
2. Wolf M, Noel GT, Stirn RJ. Investigation of the double exponential in the current—voltage characteristics of silicon solar cells. IEEE Transaction on Electron Devices. 1977;24(4):419–428. doi: https://doi.org/10.1109/T-ED.1977.18750.
3. Fahrenbruch AL, Bube RH. Fundamentals of solar cells: Photovoltaic solar energy conversion. New York–London: Academic Press; 1983. doi: https://doi.org/10.1016/B978-0-12-247680-8.X5001-4.
4. Tamrakar R, Gupta A. A review: Extraction of solar cell modelling parameters. International Journal of Innovative Research in Electrical, Electronics, Instrumentation and Control Engineering. 2015;3(1):55–60. doi: https://doi.org/10.17148/IJIREEICE.2015.3111.
5. Rhouma MBH, Gastli A. An extraction method for the parameters of the solar cell single-diode-model. 2nd European Conference on Electrical Engineering and Computer Science (EECS). 2018:433–437. doi: https://doi.org/10.1109/EECS.2018.00086.
6. Pysch D, Mette A, Glunz SW. A review and comparison of different methods to determine the series resistance of solar cells. Solar Energy Materials and Solar Cells. 2007;91(18):1698–1706.
7. Baker-Finch SC, McIntosh, KR. A freeware program for precise optical analysis of the front surface of a solar cell. 35th IEEE Photovoltaic Specialists Conference. 2010:002184–002187. doi: https://doi.org/10.1109/PVSC.2010.5616132.
8. Kołodziej A. Stability of thin film TfT's and solar cells. Krakow: AGH University of Science and Technology; 2008.
9. Kołodziej A. Staebler-Wronski effect in amorphous silicon and its alloys. Opto-Electronics Review. 2004;12(1):21–32.

10. Hinken D, Schinke C, Herlufsen S, Schmidt A, Bothe K, Brendel R. Experimental setup for camera-based measurements of electrically and optically stimulated luminescence of silicon solar cells and wafers. The Review of Scientific Instruments. 2011;83(3):1–9. doi: https://doi.org/10.1063/1.3541766.
11. Schumacher J. Numerical simulation of silicon solar cells with novel cell structures. [doctoral dissertation]. Konstanz: Universität Konstanz; 2000.
12. Merten J. Photovoltaic with amorphous silicon: Technological, physical and technical aspects. [doctoral dissertation]. Barcelona: Universitat de Barcelona; 1996.
13. Kołodziej A, Krewniak P, Nowak S. Improvements of thin silicon solar cell efficiency. Opto-Electronics Review. 2003;11(4):281–289.
14. Yang Y, Xu G, Zhang K, Zhang X, Shen H, Altermatt PP, Ver-linden PJ, Feng Z. Analysis of series resistance of industrial crystalline silicon solar cells by numerical simulation and analytical modelling. European Photovoltaic Solar Energy Conference. 2013;28:1558–1561.
15. Kołodziej A. Raport 2016 for the NCN [unpublished]. Contract no. NCN/2011/01/B/ST7/06005.
16. Kishore R. Accurate analytical expressions for the parameters of the single exponential model of the solar cells. Solid-State Electronics. 1989;32(6):493–495. doi: https://doi.org/10.1016/0038-1101(89)90032-4.
17. Fong KC, McIntosh KR, Blakers AW. Accurate series resistance measurement of solar cells. Progress in Photovoltaics. 2011;21(4):490–499. doi: https://doi.org/10.1002/pip.1216.
18. Wronski CR, von Roedern B, Kołodziej A. Thin-film Si:H-based solar cells. Vacuum: Surface Engineering, Surface Instrumentation and Vacuum Technology. 2008;82:1145–1150. doi: https://doi.org/10.1016/j.vacuum.2008.01.043.
19. Kołodziej A, Kołodziej T, Kołodziej M. Low temperature manufacturing of Si nanocrystallites in the SiOx matrix applicable in solar cells. IEEE 39th Photovoltaic Specialists Conference (PVSC). 2013: 0580-0585. doi: https://doi.org/10.1109/PVSC.2013.6744218.
20. Kołodziej A, Kołodziej M, Kołodziej T. Thin film hybrid structures perovskite and silicon photovoltaic cells. Science, Technology and Innovations. 2018;2 (1):27–30. doi: https://doi.org/10.5604/01.3001.0012.1385.